*The Institute of Space and Astronautical Science*
*Report No. 662, March 1996*

# A VOF-FCT Method for Simulating Two-Phase Flows of Immiscible Fluids

By
Ho Sang KWAK and Kunio KUWAHARA
(February 15, 1996)

**ABSTRACT** : A new numerical method is designed to simulate two-phase flows of two immiscible fluids, based on the concept of a fractional volume of fluid (VOF). An accurate advection scheme for the transport of the volume fraction is designed to trace the interface between fluids, which adopts a proper blending of the upwind and downwind fluxes according to the shape of interface. To acquire a better description of the interface motion, the time accuracy of the scheme is improved by including the cross directional upstream effects. This advection scheme is interlinked with the flux corrected transport (FCT) technique to guarantee the monotonicity in the solution. Together with the interface tracking method, an efficient solution algorithm, of the second order accuracy in time, to the Navier-Stokes equations is also constructed. Numerical tests are conducted for several benchmark problems, which illustrate the accuracy and robustness of the present method.

## 1. INTRODUCTION

Several numerical methods have been proposed to describe time-dependent flows of assemblies of immiscible fluids. These flows are characterized by the presence of interfaces, which divide the flow domain into regions of individual component fluids. The interface may be identified to be a demarcation surface across which steep changes (or discontinuities) in fluid properties exist. The free surface may be an extreme form of such interfaces, in which the density of one fluid (gas) is negligibly small in comparison to the other fluid (liquid). One overriding concern is that, throughout the flow domain, the divergence-free constraint as well as the mass continuity has to be satisfied. Oftentimes, these pose considerable difficulties in achieving a robust and efficient numerical solution procedure.

One widely-utilized numerical technique is the interface tracking method based on the Lagrangian description of the interface motion. The marker-and-cell (MAC) method [*1,2*] and the smooth particle hydrodynamics (SPH) [*3*] are prime examples. This approach enjoys the advantage of logical simplicity and it can readily be extended to three-dimensional situations. However, this method requires huge amounts of computer storage, in particular, for three-dimensional problems. In addition, difficulties are encountered in dealing with the topological changes of interface and in ensuring the global constraints of mass and momentum conservations.

Another well-established routine, termed the interface capturing method, calls for one or more additional field variables, instead of a large number of Lagrangian particles, to monitor the interface motion. For instance, in the volume of fluid (VOF) method [*4-6*], the volume fraction of a fluid, $C$, is introduced. The conservation equations for the field variables are solved by using an

advection scheme on an arbitrary Lagrangian-Eulerian mesh. The fluid interface are traced by tracking the sharp variations of $C$. This approach is capable of depicting the interface with a minimum requirement of storage. Disadvantages of this method are that numerical errors are generated by the advection scheme, which turn up in the form of non-physical numerical diffusion and/or dispersion. For a successful application of this method, therefore, an accurate advection scheme is essential to capture the discontinuities and to force them to propagate with the proper interface velocity.

The original version of VOF [*4*], for the surface sharpening, selected either the upwind (donor) flux or the downwind (acceptor) flux, depending on the evaluated shape of interface. Lafaurie et al. [*5*] recently put forward an amended advection scheme, which takes a weighted combination of the upwind and downwind fluxes. A generalized criterion was suggested in [*5*] to construct suitable advection schemes, which takes account of the directional angle of the interface normal to the flow direction. The results of these efforts were shown to yield appreciable overall improvement, especially by reducing small-scale errors known as flotsam.

It should be pointed out that the preceding advection schemes [*4,5*] are of low-order of accuracy both in time and space. Furthermore, the basic framework of the methods is grounded in a uni-directional consideration of the convection terms. Consequently, a relatively accurate depiction can be obtained of the one-dimensional interface propagation; however, for multi-dimensional problems, the method produces unphysical numerical deformations of the interface. As demonstrated by Lafaurie et al. [5], these numerical deformations include the rounding of the interface near the corner region, and large amounts of flotsam or spikes are seen on the interface under pronounced rotation effects.

The purpose of this paper is to address the above-mentioned shortcomings of the existing methodologies. The strategy here is to advance a modified-VOF method with a view toward minimizing the numerical errors inherent to the preceding versions [*4,5*]. A key ingredient of the present endeavor is to bring in the cross-directional upstream effects into the fluxing scheme. This approach will also lead to improvement of time accuracy of the advection terms. Another crucial issue of the present work is to procure a monotone algorithm. The afore-ascertained blending of the upwind and downwind schemes [*4,5*] are better suited for the surface-sharpening. However, it is also recognized that, such simplistic schemes, even if the cross-directional upstream influences are duly incorporated, do not yield monotone results; local overshoots and undershoots are included in the solution [*7*]. As a remedy, Lafaurie et al. [*5*] effectuated an explicit cut-off to maintain the value of the volume fraction within certain ranges. In the present study, as a means to ensure monotonicity, an interlink is made between the present advection scheme and the generalized flux-corrected transport (FCT) procedure [*8*]. This manipulation is compatible with pairs of lower-order (diffusive) and higher-order (antidiffusive) fluxing schemes. Furthermore, this method can easily be extended to multi-dimensional flows. In all, the original FCT due to Zalesak [*8*] will be expanded to deal with the flows of immiscible fluids.

Another objective of the study is to design a more efficient solution algorithm to the Navier-Stokes equations. An iterative implicit method, with a second-order time accuracy for the linear as well as nonlinear terms, is utilized. In summary, the main tasks of the present paper are to build an improved VOF-type methodology, which minimizes numerical errors for multi-dimensional flows and produces monotonic results, in conjunction with a more versatile Navier-Stokes solver.

## 2. TRANSPORT OF THE VOLUME FRACTION

### *2.1. Previous Advection Schemes*

Consider a flow of two immiscible fluids, fluid 1 and fluid 2, of different densities $\rho_1$ and $\rho_2$,

respectively. The traditional VOF technique introduces an additional field variable, $C$, the volume fraction of fluid 1, such that $C=1$ inside the region of fluid 1 and $C=0$ in the region of fluid 2. The density in the domain is expressed by

$$\rho=C\rho_1+(1-C)\rho_2. \tag{1}$$

The location of interface is determined by monitoring sharp variations of $C$ in the solution domain.

The equation of mass conservation of fluids is

$$\frac{\partial C}{\partial t}+\nabla\cdot(\mathbf{u}\rho)=0, \tag{2}$$

where $\mathbf{u}$ is the velocity vector. The incompressibility of both fluids enforces the divergence-free velocity field,

$$\nabla\cdot\mathbf{u}=0. \tag{3}$$

From Eqns. (1)-(3), the mass conservation of the fluid 1 becomes

$$\frac{\partial C}{\partial t}+\nabla\cdot(\mathbf{u}C)=0. \tag{4}$$

A standard finite-volume procedure on a staggered grid is employed to integrate Eq. (4). A typical two-dimensional cell configuration is shown in Fig. 1. The volume fraction $C$ is evaluated at the cell center $(i,j)$ and the horizontal velocity $u$ and the vertical velocity $v$ are defined at the vertical boundaries $(i\pm1/2,j)$ and the horizontal boundaries $(i,j\pm1/2)$, respectively.

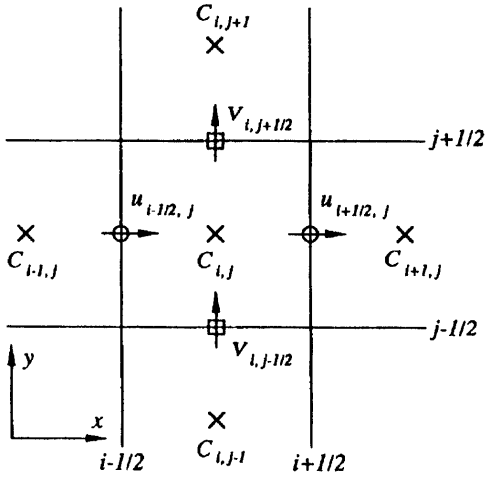


Fig. 1 Typical cell configuration.

Integration of Eq. (4) over a control volume and over the time interval $\Delta t$ yields a discretized equation,

$$(C_{i,j}^{n+1}-C_{i,j}^{n})V_{i,j}=f_{i-1/2,j}-f_{i+1/2,j}+f_{i,j-1/2}-f_{i,j+1/2}, \tag{5}$$

where $V_{i,j}$ is the volume of the cell $(i,j)$, and $n$ denotes the index for time $t_n$ such that $t_{n+1}=t_n+\Delta t$. In the above equation, $f_{i\pm1/2,j}$ and $f_{i,j\pm1/2}$ are respectively the fluxes of $C$ advected across the vertical and horizontal boundaries during the time interval $\Delta t$:

$$f_{i\pm1/2,j}=\int_{t_n}^{t_{n+1}}\int_{dA} Cu_{i\pm1/2,j}\,dA_{i\pm1/2,j}dt, \quad f_{i,j\pm1/2}=\int_{t_n}^{t_{n+1}}\int_{dA} Cv_{i,j\pm1/2}\,dA_{i,j\pm1/2}dt, \tag{6}$$

where $A_{i\pm1/2,j}$ and $A_{i,j\pm1/2}$ are the surface areas of the vertical and horizontal boundaries of the cell $(i,j)$, respectively.

As a means to define these fluxes, the upwind fluxes, $f^U_{i-1/2,j}$, $f^U_{i,j-1/2}$, and the downwind fluxes, $f^D_{i-1/2,j}$, $f^D_{i,j-1/2}$, are derived based on the donor-acceptor concept:

$$f^U_{i-1/2,j}=Q_{i-1/2,j}\cdot C^n_{i-1/2-l/2,j}, \quad f^U_{i,j-1/2}=Q_{i,j-1/2}\cdot C^n_{i,j-1/2-m/2}, \tag{7}$$

$$f^D_{i-1/2,j}=Q_{i-1/2,j}\cdot C^n_{i-1/2+l/2,j}, \quad f^D_{i-1/2}=Q_{i,j-1/2}\cdot C^n_{i,j-1/2+m/2}, \tag{8}$$

where $l=sign(Q_{i-1/2,j})$, $m=sign(Q_{i,j-1/2})$. $Q_{i-1/2,j}$ and $Q_{i,j-1/2}$ are the volume fluxes advected across the boundaries $A_{i-1/2,j}$ and $A_{i,j-1/2}$, respectively,

$$Q_{i-1/2,j}=u_{i-1/2,j}A_{i-1/2,j}\Delta t, \quad Q_{i,j-1/2}=v_{i,j-1/2}A_{i,j-1/2}\Delta t. \tag{9}$$

Obviously, in the above simple fluxing schemes, only nearest two neighboring grid points are taken into consideration. The upwind (downwind) scheme portrays correctly the interface speed when the interface is nearly parallel (perpendicular) to the flow direction. The drawback of the upwind scheme is the numerical diffusion, which tends to smear out the interface over a number of grid points. The downwind scheme enjoys the favorable surface-sharpening capability, but is prone to numerical instability.

In an effort to rectify the above-stated disadvantage of the upwind and downwind schemes, Lafaurie et al. [5] devised a fluxing scheme based on a weighted average of these two fluxes. This modified downwind flux may be represented as

$$f^{MD}_{i-1/2,j}=l\cdot\max[\tilde{f}_{i-1/2,j}, |Q_{i-1/2,j}|-(1-C^n_{i-1/2-l/2,j})V_{i-1/2-l/2,j}], \tag{10a}$$

$$f^{MD}_{i,j-1/2}=m\cdot\max[\tilde{f}_{i,j-1/2}, |Q_{i,j-1/2}|-(1-C^n_{i,j-1/2-m/2})V_{i,j-1/2-m/2}], \tag{10b}$$

where

$$\tilde{f}_{i-1/2,j}=\min[|Q_{i-1/2,j}C^n_{i-1/2+l/2,j}|, C^n_{i-1/2-l/2,j}V_{i-1/2-l/2,j}],$$

$$\tilde{f}_{i,j-1/2}=\min[|Q_{i,j-1/2}C^n_{i,j-1/2+m/2}|, C^n_{i,j-1/2-m/2}V_{i,j-1/2-m/2}].$$

Fig. 2 illustrates front sharpening feature of this modified fluxing scheme.

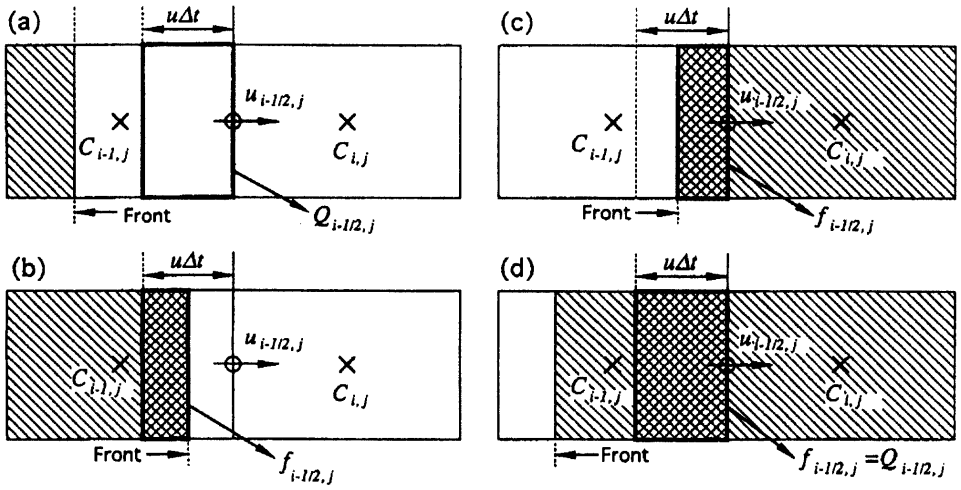


Fig. 2 Front sharpening character of the modified downwind scheme of Eq. (13) for the interface perpendicular to the flow. The single-hatched part indicates the region of fluid 1 and the cross-hatched region represents the amount of flux of fluid 1 across the cell boundary.

For a strictly one-dimensional flow, the scheme in Eq. (10) makes an accurate prediction of the motion of the interface which is perpendicular to the flow direction. For the interface which is parallel to the flow, however, this scheme causes wrinkles to create spikes on the interfaces. As a remedy, Lafaurie et al. [5] put forward a criterion to choose between a conventional upwind scheme and the modified downwind scheme of Eq. (10). The idea was to select a proper fluxing scheme in light of the relative orientation of the interface, i.e., the downwind (upwind) scheme is selected when the interface is mainly perpendicular (parallel) to the flow direction. To this end, the directional angles of the interface with respect to the $x$ and $y$ directions as

$$\theta^x = \arccos(|n^x|), \qquad \theta^y = \arccos(|n^y|), \tag{11}$$

where $n^x$ and $n^y$ are, respectively, the x- and y-components of unit normal vector to the interface, $\mathbf{n}$, (see Fig. 3)

$$\mathbf{n} = \nabla C / |\nabla C|. \tag{12}$$

Then, the resulting fluxing method becomes

$$f_{i-1/2,j} = \begin{cases} f^{MD}_{i-1/2,j}, & \text{for } \theta^x < \theta^y \\ f^{U}_{i-1/2,j}, & \text{for } \theta^x \geq \theta^y \end{cases}, \qquad f_{i,j-1/2} = \begin{cases} f^{MD}_{i,j-1/2}, & \text{for } \theta^x < \theta^c \\ f^{U}_{i,j-1/2}, & \text{for } \theta^y \geq \theta^c \end{cases}, \tag{13}$$

where $\theta^c$ denotes the reference angle for the choice of the fluxing schemes. The optimal values of $\theta^c$ were suggested $1.0 < \theta^c < 1.05$ [5].

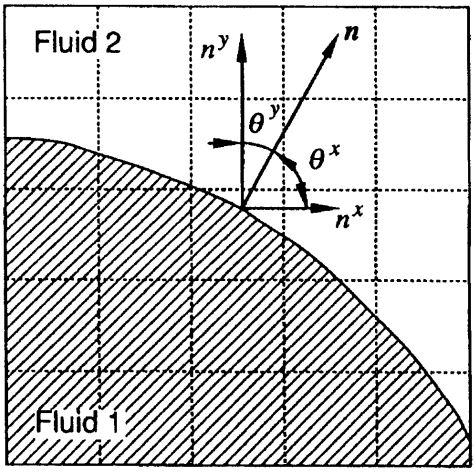


Fig. 3 The directional angle of the interface.

### 2.2. *The Fluxing Scheme Including Cross-Directional Upstream Effects*

For one-dimensional flows, the scheme of Eq. (13) accurately depicts the behavior of the interface. This scheme, however, suffers from undesirable numerical errors in multi-dimensional situations. Fig. 4 is illustrative of such interface deformation. A two-dimensional square domain filled with fluid 1 is propagated in a uniform flow field $(u,v)=(1,1)$ during a unit time step $\Delta t=\Delta x/u=\Delta y/v=0.5$. It is evident that a straightforward application of the advection scheme of Eq. (13) give rise to distortions in the corner regions, as exemplified in the circle surrounding A and B in Fig. 4(a). Another type of numerically-generated interface deformation may be found when a rectangular domain is rotated [5]. These numerical errors turn up in the form of large amounts of flotsam on large lattice and/or spike-like spatial zigzag oscillations on the rectangular surfaces. These anomalies are attributed to the facts that the scheme is constructed based on a one-dimensional-like representation of the flux terms by taking into account only two neighbors points.

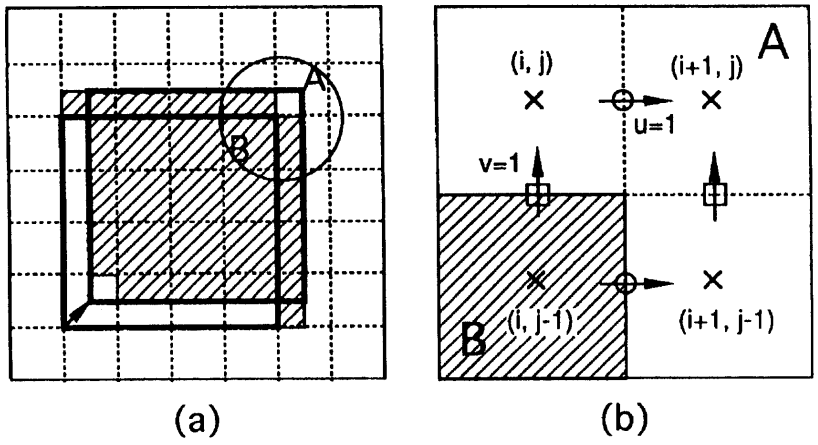


Fig. 4 Example of pure propagation of a square domain in a velocity field $(u,v)=(1,1)$. The heavy lines in the figures indicate the initial condition and the exact solution after a time step, $\Delta t=0.5\Delta x/u$. The hatched area in frame (a) represents the numerically acquired solution by Eq. (13). Fig. 4(b) shows an enlarged view of the frame (a) near the leading edge of the square.

In order to minimize these errors, the numerical accuracy has to be enhanced, and one significant approach is to bring forth the cross-directional upstream effects in designing the advection scheme. Fig. 4(b) provides an enlarged view of the corner area of the rectangle of Fig. 4(a). If a direct application of the advection scheme of Eq. (13), cell A does not feel the impact of cell B, since all the fluxes advected into cell A do not contain any information of cell B which is in a cross-directionally upstream location. Consequently, the corner area in Fig. 4(a) undergoes distortions. These numerically-generated inaccuracies, therefore, may be ameliorated if the effects of cross-directional upstream cells are properly accounted for in the numerical descriptions of the interface. Toward this end, this paper aims to propose a fluxing scheme which will make an improved portrayal of the interface.

Before proceeding further, it is convenient to define fluxing operators :

$$F(Q_x,C_{a,j},V_{a,j},\theta^x_{a,j})=\begin{cases} Q_x\cdot C_{a-l/2,} & \text{for } \theta^x_{a-l/2,j} \geq \theta^c \\ l\cdot\max[\tilde{F}_{a,j}, \mid Q_x \mid -(1-C_{a-l/2,j})V_{a-l/2,j}], & \text{for } \theta^x_{a-l/2,j} < \theta^c \end{cases}, \tag{14a}$$

$$F(Q_y,C_{i,b},V_{i,b},\theta^y_{i,b})=\begin{cases} Q_x\cdot C_{i,b-m/2,} & \text{for } \theta^y_{i,b-m/2} \geq \theta^c \\ m\cdot\max[\tilde{F}_{i,b}, \mid Q_y \mid -(1-C_{i,b-m/2})V_{i,b-m/2}], & \text{for } \theta^y_{i,b-m/2} < \theta^c \end{cases}, \tag{14b}$$

where

$$\tilde{F}_{a,j}=\min[Q_xC_{a+l/2,j},C_{a-l/2,j}V_{a-l/2,j}], \quad \tilde{F}_{i,b}=\min[Q_yC_{i,b+m/2},C_{i,b-m/2}V_{i,b-m/2}],$$

in which $l=sign(Q_x)$, $m=sign(Q_y)$. Then, Eq. (13) can be rewritten as

$$f_{i-1/2,j}=\mathrm{F}(Q_{i-1/2,j},C^n_{i-1/2,j},V_{i-1/2,j},\theta^x_{i-1/2,j}), \tag{15a}$$

$$f_{i,j-1/2}=\mathrm{F}(Q_{i,j-1/2},C^n_{i,j-1/2},V_{i,j-1/2},\theta^x_{i,j-1/2}). \tag{15b}$$

Now, the cross-upstream effects are brought into the advection scheme. Consider a cell $(i,j)$ and assume positive velocities at the right and bottom boundaries of this cell, i.e., $u_{i+1/2,j}>0$ and $v_{i,j-1/2}>0$. In the usual advection schemes of Eqs. (7), (8), and (13), only the local effects from cells $(i,j)$ and $(i+1,j)$ affect the flux $f_{i+1/2,j}$. In fact, during $\Delta t$, the effects from the cross-directional upstream cell $(i,j\text{-}1)$ are transported via volume flux $Q_{i,j-1/2}$. In order to make a more accurate depiction of the flux of $C$ from the cell $(i,j)$ to the cell $(i+1,j)$, the impact from the cross-directional upstream cell $(i,j\text{-}1)$ should be included in the flux $f_{i+1/2,j}$. Fig. 5 portrays the baseline idea.

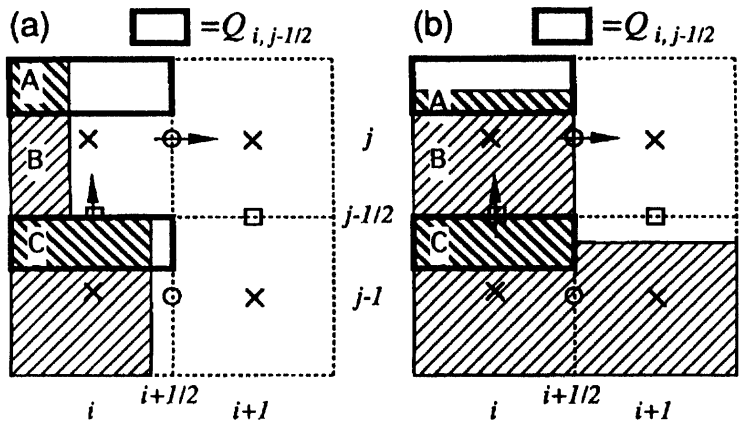


Fig. 5 Two examples for describing the mechanism to put the cross-directional effects into the flux. (a) For a nearly vertical interface, (b) for a nearly horizontal interface. The hatched regions indicate the domain filled with fluid 1.

Consider the vertical transport of $C$ from the cell $(i,j\text{-}1)$ to the cell $(i,j)$ by $Q_{i,j\text{-}1/2}(>0)$. The volume occupied by fluid 1 in the cell $(i,j)$ at time $t=t_n$ is represented by the region (A+B) in Fig. 5. Allowing a strictly one-dimensional transport due to $Q_{i,j\text{-}1/2}$, the volume of fluid 1 in the cell $(i,j)$ at time $t=t_{n+1}$ becomes the area of the region (B+C). Thus, a second-order approximation of $C$ in time can be estimated as

$$C_{i,j}^{n+1/2} \approx (C^{A+B}+C^{B+C})/2=(C_{i,j}^{n}+C^{B+C})/2. \tag{16}$$

The area of C is equivalent to the amount of the volume fraction advected into the cell $(i,j)$ from the lower cell $(i,j\text{-}1)$ during $\Delta t$ via $Q_{i,j\text{-}1/2}$. By using the fluxing operator of Eq. (14), this can be expressed as

$$f_{i,j}^{B+} = \alpha_{i,j}^{B} F(Q_{i,j-1/2}, C_{i,j-1/2}^{n}, V_{i,j-1/2}, \theta^{y}{}_{i,j-1/2}), \tag{17}$$

where $\alpha_{i,j}^{B}=\max[0,sign(Q_{i,j\text{-}1/2})]$. The remaining task is to calculate the area of B, which can be readily accomplished by subtracting the area of A from the area of (B+C). The area of A can be interpreted to be the amount of the volume fraction advected out to the upper cell $(i,j+1)$ from the cell $(i,j)$ due to $Q_{i,j\text{-}1/2}$. This quantity can be determined as

$$f_{i,j}^{B-} = \alpha_{i,j}^{B} F(Q_{i,j-1/2}, C_{i,j+1/2}^{n}, V_{i,j+1/2}, \theta^{y}{}_{i,j+1/2}). \tag{18}$$

The volume fraction of the cell $(i,j)$ at an intermediate time step, containing the impact of vertical transport from the bottom cell $(i,j-1)$, becomes

$$C_{i,j}^{n+1/2} \approx \frac{2C_{i,j}^{n}+(f_{i,j}^{B+}-f_{i,j}^{B-})/V_{i,j}}{2}. \tag{19}$$

Consequently, the horizontal flux $f_{i+1/2,j}$ is evaluated by using the value of $C_{i,j}^{n+1/2}$, which indicates the proper presence of the cross-directional upstream effects. It is noted that the key elements of the present methodology are linked to temporally second-order approximation of the convective flux terms.

The above-described idea to put the cross-directional upstream contributions into the fluxes can be extended to general situation. Now, consider all the positive volume fluxes advected into the cell $(i,j)$ from the neighbor cells. The vertical flux of $C$ advected into the cell $(i,j)$ from the upper cell due to a negative volume flux at the top boundary $Q_{i,j+1/2}(<0)$ and the associated flux advected out of the cell $(i,j)$ to the lower cell $(i,j\text{-}1)$ can be estimated, in a similar way,

$$f_{i,j}^{T+} = \alpha_{i,j}^{T} F(Q_{i,j+1/2}, C_{i,j+1/2}^{n}, V_{i,j+1/2}, \theta^{y}{}_{i,j+1/2}), \tag{20}$$

$$f_{i,j}^{T-} = \alpha_{i,j}^{T} F(Q_{i,j-1/2}, C_{i,j-1/2}^{n}, V_{i,j-1/2}, \theta^{y}{}_{i,j-1/2}), \tag{21}$$

where $\alpha_{i,j}^{T}=\min[0,sign(Q_{i,j+1/2})]$. Likewise, the contributions of the horizontal fluxes advected into the cell $(i,j)$ from the left and right vertical boundaries can be evaluated,

$$f_{i,j}^{L+} = \alpha_{i,j}^{L} F(Q_{i-1/2,j}, C_{i-1/2,j}^{n}, V_{i-1/2,j}, \theta^{x}{}_{i-1/2,j}), \tag{22}$$

$$f_{i,j}^{L+} = \alpha_{i,j}^{L} F(Q_{i-1/2,j}, C_{i+1/2,j}^{n}, V_{i+1/2,j}, \theta^{x}{}_{i+1/2,j}), \tag{23}$$

$$f_{i,j}^{R+} = \alpha_{i,j}^{R} F(Q_{i+1/2,j}, C_{i+1/2,j}^{n}, V_{i+1/2,j}, \theta^{x}{}_{i+1/2,j}), \tag{24}$$

$$f_{i,j}^{R+} = \alpha_{i,j}^{R} F(Q_{i+1/2,j}, C_{i-1/2,j}^{n}, V_{i-1/2,j}, \theta^{x}{}_{i-1/2,j}), \tag{25}$$

where $\alpha^L_{i,j}=\max[0,sign(Q_{i-1/2,j})]$, $\alpha^R_{i,j}=\min[0,sign(Q_{i+1/2,j})]$.

Here, two temporary volume fractions at an intermediate time step $n+1/2$ are defined. These contain the effects of vertical and horizontal transports of the volume fraction from the upstream cells, respectively:

$$C^Y_{i,j}=C^n_{i,j}+(f^{B+}_{i,j}-f^{B-}_{i,j}+f^{T+}_{i,j}-f^{T-}_{i,j})/(2V_{i,j}), \tag{26a}$$

$$C^X_{i,j}=C^n_{i,j}+(f^{L+}_{i,j}-f^{L-}_{i,j}+f^{R+}_{i,j}-f^{R-}_{i,j})/(2V_{i,j}). \tag{26b}$$

Finally, the horizontal and vertical fluxes of $C$ are determined by using the values $C^Y_{i,j}$ and $C^X_{i,j}$, respectively. Therefore, the present fluxing scheme yields

$$f^*_{i-1/2,j}=F(Q_{i-1/2,j},C^Y_{i-1/2,j},V_{i-1/2,j},\theta^x_{i-1/2,j}), \tag{27a}$$

$$f^*_{i,j-1/2}=F(Q_{i-1/2,j},C^X_{i,j-1/2},V_{i,j-1/2},\theta^y_{i,j-1/2}). \tag{27b}$$

Note the difference between Eq. (15) and Eq. (27) in that $C^n_{i,j}$ is replaced by $C^Y_{i,j}$ and $C^X_{i,j}$ to incorporate the cross-directional upstream influences. It is important to point out that $C^Y_{i,j}$ and $C^X_{i,j}$ differ from the values of $C$ acquired by applying directional-splitting of the one-dimensional advection scheme [*9*] which generates a directional bias. The present method employs $C^Y_{i,j}$ and $C^X_{i,j}$ so that the effects advected from the cross-directional upstream are duly included in the fluxes while maintaining the surface-sharpening nature of the fluxing scheme. The procedures in Eqs. (17)-(27) are free from a directional bias, and, extension to the three-dimensional situations is straightforward.

### *2.3 Coupling with the FCT Algorithm for Monotonicity*

The essential aspect of advection algorithms of Eqs. (13) and (27) is a judicious blending of the upwind and downwind schemes, and the front-sharpening feature is originated from the downwind fluxing. The antidiffusive nature of the downwind scheme is useful for interface-capturing, but it leads to a defect that the monotonic solution is not guaranteed. This is true for the present fluxing scheme as well as for the previous schemes [*4,5*]. Since VOF uses a conservative formulation of the flux terms, conservation of $C$ is satisfied in the full computational domain if the divergence-free condition is in effect. However, a non-monotone advection scheme can generate locally-unphysical overshoots and undershoots [*7*]; in the present situations, local extrema in the solution of $C$ greater than 1 or less than 0 may be created. In order to prevent such a deficiency, Lafaurie et al. [*5*] executed a cut-off filtering in calculating the fluxes, such that $C$ should be bounded between 0 and 1. This artificial cut-off can, in turn, result in a local gain or loss of the fluid volume. In the present study, a more physically-reasonable method is explored to realize the monotonicity.

The flux-corrected transport (FCT) is a technique to achieve both the monotonicity and the accuracy of an advection scheme which are mutually-exclusive [*8-10*]. The basic idea of FCT is the two-step evaluation of the advection terms; first, a fully-diffusive monotonic solution is acquired, and subsequently a higher-order antidiffusive flux is superposed to the fully-diffusive solution to reduce numerical diffusion. Among others, the generalized formulation of FCT by Zalesak [*8*] has several attractive features. First, this formulation is essentially multi-dimensional, which produces no directional bias. This implies an easy application to multi-dimensional flows, in which the

directional splitting of FCT [9] remedied the problems in flows of nearly or fully incompressible fluids. More appealing is the generality of the formulation that monotonicity can be ensured by using combinations of diffusive lower-order and accurate higher-order advection schemes.

The general procedures of Zalesak's FCT are :

(1) Compute $f^L_{i-1/2,j}$ and $f^L_{i,j-1/2}$, i.e., the transportive fluxes by a lower-order algorithm, which guarantees monotonic results.

(2) Compute $f^H_{i-1/2,j}$ and $f^H_{i,j-1/2}$, i.e., the transportive fluxes by a higher-order algorithm which results in a more accurate solution, but which can lead to physically unacceptable over- and/or undershoots in the solution.

(3) Compute the updated lower-order, transported and diffused solution,

$$C^{td}_{i,j}=C^n_{i,j}+(f^L_{i-1/2,j}-f^L_{i+1/2,j}+f^L_{i,j-1/2}-f^L_{i,j+1/2})/V_{i,j}. \tag{28}$$

(4) Define the antidiffusive fluxes,

$$f^{ad}_{i-1/2,j}=f^H_{i-1/2,j}-f^L_{i-1/2,j},\quad f^{ad}_{i,j-1/2}=f^H_{i,j-1/2}-f^L_{i,j-1/2}. \tag{29}$$

(5) Limit the antidiffusive fluxes $f^{ad}_{i-1/2,j}$ and $f^{ad}_{i,j-1/2}$, so that the solution at the advanced time is free of the newly-generated overshoots and undershoots,

$$f^c_{i-1/2,j}=\beta_{i-1/2,j}f^{ad}_{i-1/2,j},\quad f^c_{i,j-1/2}=\beta_{i,j-1/2}f^{ad}_{i,j-1/2}. \tag{30}$$

(6) Apply the limited antidiffusive fluxes to obtain new values, $C^{n+1}_{i,j}$,

$$C^{n+1}_{i,j}=C^n_{i,j}+(f^c_{i-1/2,j}-f^c_{i+1/2,j}+f^c_{i,j-1/2}-f^c_{i,j+1/2})/V_{i,j}. \tag{31}$$

Step 5 is the flux limiting phase which ensures that the antidiffusive correction does not generate the unphysical overshoots and undershoots. The flux limiting method of Zalesak is accomplished by defining the following six quantities:

$$P^+_{i,j}=\max(0,f^{ad}_{i-1/2,j})-\min(0,f^{ad}_{i+1/2,j})+\max(0,f^{ad}_{i,j-1/2})-\min(0,f^{ad}_{i,j+1/2}), \tag{32}$$

$$S^+_{i,j}=(C^{\max}_{i,j}-C^{td}_{i,j})V_{i,j}, \tag{33}$$

$$R^+_{i,j}=\begin{cases}\min(1,S^+_{i,j}/P^+_{i,j}), & \text{for } P^+_{i,j}>0\\ 0, & \text{for } P^+_{i,j}=0\end{cases}, \tag{34}$$

$$P^-_{i,j}=\max(0,f^{ad}_{i+1/2,j})-\min(0,f^{ad}_{i-1/2,j})+\max(0,f^{ad}_{i,j+1/2})-\min(0,f^{ad}_{i,j-1/2}), \tag{35}$$

$$S^-_{i,j}=(C^{td}_{i,j}-C^{min}_{i,j})V_{i,j}, \tag{36}$$

$$R^-_{i,j}=\begin{cases}\min(1,S^-_{i,j}/P^-_{i,j}), & \text{for } P^-_{i,j}>0\\ 0, & \text{for } P^-_{i,j}=0\end{cases}. \tag{37}$$

Note that $R^+_{i,j}$,and $R^-_{i,j}$ are the least–value upper bounds on the fraction. These must multiply all antidiffusive fluxes, into and away from the cell $(i,j)$, to guarantee that there is no unphysical overshoots and undershoots in the cell $(i,j)$. Consequently, to ensure that there are no overshoots and undershoots in the full domain, it is required

$$\beta_{i-1/2,j}=\begin{cases}\min(R^{+}_{i,j},R^{-}_{i-1,j}), \text{ for } f^{ad}_{i-1/2,j}\geq 0\\ \min(R^{-}_{i,j},R^{+}_{i-1,j}), \text{ for } f^{ad}_{i-1/2,j}<0\end{cases}, \qquad \beta_{i,j-1/2}=\begin{cases}\min(R^{+}_{i,j},R^{-}_{i-1,j}), \text{ for } f^{ad}_{i,j-1/2}\geq 0\\ \min(R^{-}_{i,j},R^{+}_{i,j-1}), \text{ for } f^{ad}_{i,j-1/2}<0\end{cases}. \tag{38}$$

The incompressibility of the fluids provides a natural choice for the quantities $C^{\max}_{i,j}$, and $C^{\min}_{i,j}$:

$$C^{\max}_{i,j}=\max(C^{n}_{l,m},C^{td}_{l,m}), \tag{39}$$

$$C^{\min}_{i,j}=\min(C^{n}_{l,m},C^{td}_{l,m}), \tag{40}$$

for $l=i-1,i,i+1$ and $m=j-1,j,j+1$. Note that, in contrast to the original method of Zalesak, Eqs. (39) and (40) take into account four additional points. This is in line with the advection scheme of Eq. (27), which contains the cross-directional upstream contributions.

The afore-mentioned advection scheme of Eq. (27) is now coupled with Zalesak's FCT. It is recalled that, although the cross-directional upstream effects are included, the advection scheme of Eq. (27) consists of two basic fluxing schemes, i.e., the diffusive upwind scheme and the modified downwind scheme of antidiffusive nature. It is then advantageous to treat the flux given by the upwind scheme as the diffusive flux, and to define the flux given by the modified downwind scheme of Eq. (27) as the higher-order flux,

$$f^{L}_{i-1/2,j}=f^{U}_{i-1/2,j}=Q_{i-1/2,j}C^{Y}_{i-1/2-l/2,j}, \quad f^{L}_{i,j-1/2}=f^{U}_{i,j-1/2}=Q_{i,j-1/2}C^{X}_{i,j-1/2-m/2}, \tag{41}$$

$$f^{H}_{i-1/2,j}=f^{*}_{i-1/2,j}, \quad f^{H}_{i,j-1/2}=f^{*}_{i,j-1/2}. \tag{42}$$

The Zalesak's generalized FCT algorithm can be utilized by using the above fluxes. However, the flux limiting of Eqs. (32)-(40) still yields excessive numerical diffusion in multi-dimensional situations. Note that, due to the characteristics of the upwind and downwind fluxes, near the interface region, $O(f^{L}_{i,j-1/2})\sim O(f^{ad}_{i,j-1/2})$. The flux limiting of (32)-(40) is basically a one-through-step method biased to the strategy of guaranteeing a monotone solution. This method does not provide sufficient antidiffusion to be applicable without violating the monotonicity; rather, it gives only a minimal antidiffusion. In order to satisfy both the constraints of the surface-sharpening character and the monotonicity, an appropriate method to reduce excessive numerical diffusion should be devised. For this purpose, an alternative approach is considered; steps 3 - 6 in the above procedure of Zalesak are replaced by the following iterative routine :

(3') Define the iterative transported monotonic solution,

$$C^{td(k+1)}_{i,j}=C^{n+1(k)}_{i,j}. \tag{43}$$

(4') Compute the iterative antidiffusive fluxes,

$$f^{ad(k+1)}_{i-1/2,j}=(1-\beta^{(k)}_{i-1/2,j})f^{ad(k)}_{i-1/2,j}, \quad f^{ad(k+1)}_{i,j-1/2}=(1-\beta^{(k)}_{i,j-1/2})f^{ad(k)}_{i,j-1/2}. \tag{44}$$

(5') Limit the iterative antidiffusive fluxes $f^{ad}_{i-1/2,j}$ and $f^{ad}_{i,j-1/2}$,

$$f^{c(k+1)}_{i-1/2,j}=\beta^{(k+1)}_{i-1/2,j}f^{ad(k+1)}_{i-1/2,j}, \quad f^{c(k+1)}_{i,j-1/2}=\beta^{(k+1)}_{i,j-1/2}f^{ad(k+1)}_{i,j-1/2}. \tag{45}$$

(6') Compute $C^{n+1}_{i,j}$ at the advanced time step,

$$C^{n+1(k+1)}_{i,j}=C^{td(k+1)}_{i,j}+(f^{c(k+1)}_{i-1/2,j}-f^{c(k+1)}_{i+1/2,j}+f^{c(k+1)}_{i,j-1/2}-f^{c(k+1)}_{i,j+1/2})/V_{i,j}. \tag{46}$$

In the above, $k$ denotes the iteration level. The values at the zero-iteration step are given as

$$C_{i,j}^{n+1(0)}=C_{i,j}^{n}+(f_{i-1/2,j}^{L}-f_{i+1/2,j}^{L}+f_{i,j-1/2}^{L}-f_{i,j+1/2}^{L})/V_{i,j}, \tag{47}$$

$$f_{i-1/2,j}^{ad(0)}=f_{i-1/2,j}^{H}-f_{i-1/2,j}^{L},\ f_{i,j-1/2}^{ad(0)}=f_{i,j-1/2}^{H}-f_{i,j-1/2}^{L}, \tag{48}$$

$$\beta_{i-1/2,j}^{(0)}=\beta_{i,j-1/2}^{(0)}=0. \tag{49}$$

The iteration is performed until the relative variations between two successive iteration steps fall below a prescribed convergence limit,

$$|C_{i,j}^{n+1(k+1)}-C_{i,j}^{n+1(k)}|<\varepsilon. \tag{50}$$

In the above, $\beta_{i-1/2,j}^{(k+1)}$ and $\beta_{i,j-1/2}^{(k+1)}$ are evaluated by using the iterative values as in Eqs. (32)-(40). Note that this iteration do not create new maxima or minima since the antidiffusive fluxes are limited not to exceed the upper and lower bounds to ensure the monotonic solution at each iteration step. Only a right amount of the antidiffusive flux, which does not produce new maxima and minima but was not included in the previous iteration step, is considered in the new iteration step. This method becomes identical to the original FCT of Zalesak when $k$=1.

## 3. SOLVER TO THE NAVIER-STOKES EQUATIONS

In many respects of VOF, a solver to the Navier-Stokes equations constitutes a separate part, which can be pursued independently of the interface-capturing described in the previous section. In this section, a proposal is made of a solution algorithm to the Navier-Stokes equation which has the second-order accuracy in time.

Consider viscous flows of two incompressible fluids, with the surface tension effect present on the fluid interfaces. For simplicity, the properties of each fluid and the coefficient of surface tension s are assumed to be constant. The governing equations are the Navier-Stokes equations for incompressible fluids in a conservative form,

$$\frac{\partial \mathbf{u}}{\partial t}+\nabla\cdot(\mathbf{u}\otimes\mathbf{u})=-\frac{\nabla p}{\rho}+\frac{1}{\rho}\nabla\cdot\mu\nabla\mathbf{u}+\frac{1}{\rho}\sigma\kappa\delta_s\mathbf{n}, \tag{51}$$

where $\rho$ is the density, $\mu$ the dynamic viscosity, $p$ the pressure. The last term in the above equation is the capillary force acting on the fluid interface between the two fluids; $\kappa$ is the mean curvature of the interface, $\mathbf{n}$ the unit normal vector to the interface and $\delta_S$ is a delta function concentrated on the interface. The divergence-free condition of Eq. (3) and the conservation equation for $C$ of Eq. (4) are to be satisfied. The fluid properties are expressible by the volume fraction $C$,

$$\phi=\phi_1 C+\phi_2(1-C), \tag{52}$$

where $\phi$ stands for $\rho$ or $\mu$.

Eq. (51) is converted to a discretized form on a staggered grid,

$$\frac{\mathbf{u}^{n+1}-\mathbf{u}^{n}}{\Delta t}=-\mathbf{G}(\mathbf{u})+\mathbf{S}-\frac{1}{\rho}\nabla p, \tag{53}$$

where $\mathbf{G}(\mathbf{u})$ represents the nonlinear advection term and $\mathbf{S}$ includes the diffusion term, the capillary terms, and the other source terms. These terms are dealt with by a standard finite-volume

approximation. In order to solve Eq. (53), together with the Eqs. (3) and (4), a conventional predictor-corrector procedure, based on the Euler explicit time differencing, is considered.

First, the predicted velocity field $\mathbf{u}^*$, by using the known pressure field at the previous time, is calculated :

$$\frac{\mathbf{u}^* - \mathbf{u}^n}{\Delta t} = -\mathbf{G}(\mathbf{u}) + \mathbf{S} - \frac{1}{\rho}\nabla p^n. \tag{54}$$

Then, the solution at the advanced time step is obtained by using the pressure correction, $p'$,

$$\frac{\mathbf{u}^{n+1} - \mathbf{u}^*}{\Delta t} = -\frac{1}{\rho}\nabla p', \tag{55}$$

$$p^{n+1} = p^n + p', \tag{56}$$

where $p'$ is chosen so that the divergence-free condition at the advance time step is satisfied:

$$\nabla \cdot \mathbf{u}^{n+1} = 0. \tag{57}$$

Thus, the Poisson equation to find $p'$ is derived as

$$\nabla \cdot \left(\frac{\Delta t}{\rho}\nabla p'\right) = \nabla \cdot \mathbf{u}^*. \tag{58}$$

Finally, the transport equation for the volume fraction is solved following the method described in the previous section.

The above approach based on the Euler explicit method is relatively simple and straightforward. The preceding versions of VOF [*4,5*] used the MAC method as the solution algorithm to the Navier-Stokes equations, which were also based on the Euler explicit representation of the equation terms. Consequently, these methods have a first order-accuracy in time. The more challenging issue is the severe restriction of the time increment $\Delta t$; $\Delta t$ should be kept less than the values suggested from both the CFL condition and the diffusive time limit for numerical stability.

In the present study, a method of second-order time accuracy is examined to alleviate these problems. To this end, the terms in the right hand side of Eq. (53) are estimated at an intermediate time level $t_{n+1/2}$ by taking a temporal average,

$$\mathbf{G}^{n+1/2}(\mathbf{u}) = [\,\mathbf{G}^n(\mathbf{u}^n) + \mathbf{G}^{n+1}(\mathbf{u}^{n+1})\,]/2, \tag{59}$$

$$\mathbf{S}^{n+1/2} = [\mathbf{S}^n + \mathbf{S}^{n+1}]/2. \tag{60}$$

In this process, the presence of nonlinear terms $\mathbf{G}(\mathbf{u})$ poses difficulties in the numerical formulation. Here, an iterative procedure is considered to avoid difficulties stemming from the nonlinearity. The overall solution procedures are as follows:

First, a predicted velocity field is obtained by

$$\frac{\mathbf{u}^{*(k)} - \mathbf{u}^n}{\Delta t} = -\mathbf{G}^{n+1/2(k)}(\mathbf{u}) + \mathbf{S}^{n+1/2} - \frac{1}{\rho}\nabla p^{(k-1)}. \tag{61}$$

where $k$ denotes the iteration index. The nonlinear advection terms can be linearized by using the previous iteration values

$$\mathbf{G}^{n+1/2(k)}(\mathbf{u}) = [\,\mathbf{G}^n(\mathbf{u}^n) + \mathbf{G}^{n+1}(\mathbf{u}^{n+1(k-1)})\,]/2. \tag{62}$$

The next step is to secure the updated solution by using the pressure correction,

$$\frac{\mathbf{u}^{n+1(k)}-\mathbf{u}^{*(k)}}{\Delta t}=-\frac{1}{\rho}\nabla p', \tag{63}$$

$$p^{n+1(k)}=p^{n+1(k-1)}+p', \tag{64}$$

where $p'$ satisfies

$$\nabla\cdot\mathbf{u}^{n+1(k)}=0. \tag{65}$$

Thus

$$\nabla\cdot(\frac{\Delta t}{\rho}\nabla p')=\nabla\cdot\mathbf{u}^{*(k)}. \tag{66}$$

The final step is to solve the transport equation of the volume fraction $C$ as described in the previous section by using the acquired velocity field, $\mathbf{u}^{n+1/2}$

$$\mathbf{u}^{n+1/2(k)}=[\mathbf{u}^{n}+\mathbf{u}^{n+1(k)}]/2. \tag{67}$$

The iteration is repeated until the relative difference of the solutions between two successive iteration levels falls below a prescribed value. Note that the present method is designed to guarantee the divergence-free velocity field at each iteration level. In order to facilitate the convergency of this iteration procedure, educated initial guesses for $\mathbf{u}^{n+1(0)}$ and $p^{n+1(0)}$ in Eqs. (62) and (64) are needed. Due to the existence of the pressure correction step, it is natural to set

$$p^{n+1(0)}=p^{n}. \tag{68}$$

For $\mathbf{u}^{n+1(0)}$, the velocity obtained by a fully explicit calculation is selected for fast convergency,

$$\frac{\mathbf{u}^{n+1(0)}-\mathbf{u}^{n}}{\Delta t}=-\mathbf{G}^{n}(\mathbf{u}^{n})+\mathbf{S}^{n}-\frac{1}{\rho}\nabla p^{n}. \tag{69}$$

The present method has a second-order accuracy in time. The semi-implicit formulation requires matrix inversions for the momentum equations as well as for the pressure Poisson equation, and the iterative approach calls for an additional computation time. However, the advantage is the less severe restriction on $\Delta t$ caused by the diffusion time limit. The CFL condition still restricts the size of $\Delta t$, which originates from the demand to obtain a correct description of the interface behavior. A number of tests have been carried out, and it turned out that only 3-4 iterations are sufficient to produce converged solutions.

## 4. VERIFICATION TESTS

The present method consists of two major parts: one is the monotone advection scheme for the volume fraction which contains the cross-directional upstream effects, and the other is the solution algorithm to the Navier-Stokes equations which has the second-order accuracy in time. In order to demonstrate the improved features of the present advection scheme, test problems are selected which would illustrate the accuracy and robustness of the present method in depicting the interface.

### 4.1. Interface Propagation

Test problems of Lafaurie et al. [5] considering the propagation of the interface with a given velocity field, are reproduced.

In the first, consider a 10x10 square domain of cells having a uniform spacing $\Delta x=\Delta y=1$, and suppose it propagates diagonally in a uniform velocity field $(u,v)=(1,1)$. Results at time 50 sec are obtained by applying the present advection scheme, and they are compared with those by Eq. (13). Fig. 6 shows contour values of $C$, 0.05, 0.4, 0.6, 0.95. The result of the previous method given by Eq. (13) displays noticeable distortion near the corner regions. The computational results of the present method shown in Figs. 6 (b), (c), (d) demonstrate improved features near the corner regions. It is evident that the present advection scheme generates less numerical diffusion.

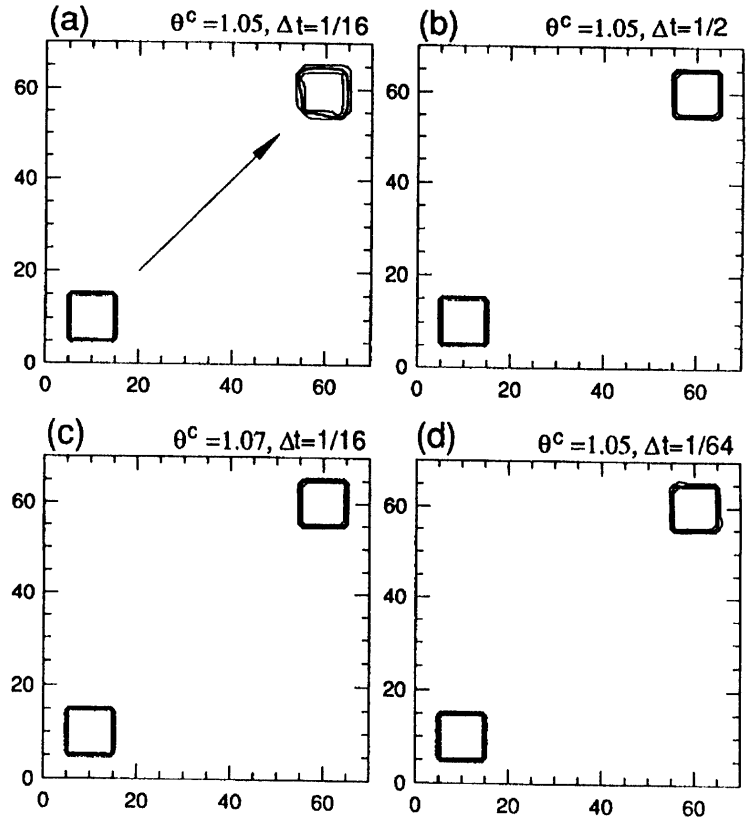


Fig. 6 Pure propagation of a square cell (a) by the preceding advection scheme of Eq. (13), and (b), (c), (d) by using the present advection scheme.

Tests were also performed by varying and critical angle $\theta^c$ and the time step, i.e., the Courant number, $Co=u\Delta t/\Delta x$. Fig. 7 shows the relative error evaluated in the form

$$E=\frac{\sum_i \sum_j |C^e_{i,j}-C^{ns}_{i,j}|}{\sum_i \sum_j |C^e_{i,j}|}, \tag{70}$$

where the superscripts $e$ and $ns$ denote the exact solution and the numerical solution, respectively. It is worth pointing out that, owing to the timely second-order formulation, the present advection scheme illustrates a better trend on $Co$. It is recalled that, as demonstrated in Fig. 4, the advection scheme of Eq. (13) is sensitive to $Co$, and the numerical error increases with $Co$ even when $Co<1$.

Fig. 7 suggests the optimal value of the critical angle, $1.05 \leq \theta^c \leq 1.10$.

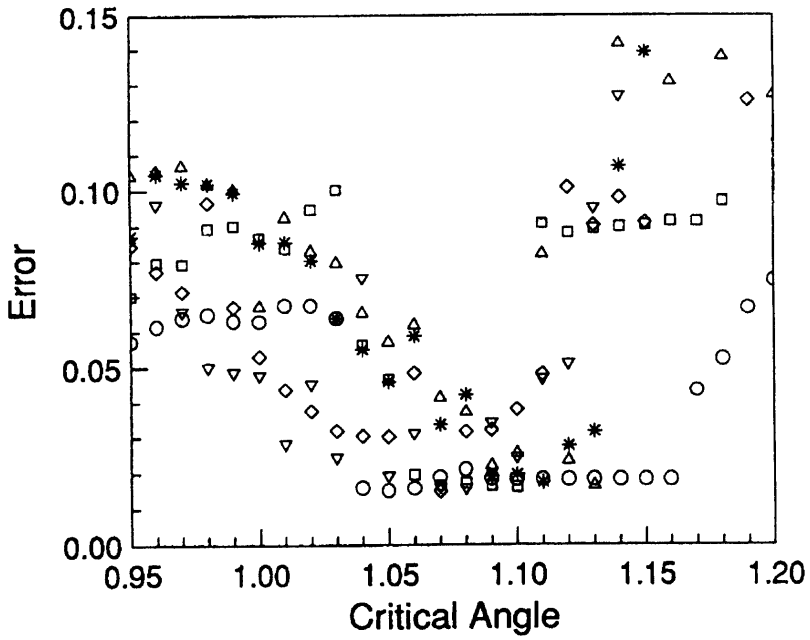


Fig. 7 Effects of the critical angle, $\theta^C$ and the Courant number, $Co=u\Delta t/\Delta x$, on numerical error generation. For the pure propagation of a square cell, numerical errors of Eq. (70) are evaluated at $t$=50.0. O, $Co$=1/2; □, $Co$=1/4; Δ, $Co$=1/8; ◇, $Co$=1/16; ∇, $Co$=1/32; ∗, $Co$=1/64.

Another test problem is the rotation of a 30x10 rectangular domain on a uniform grid, for which numerical experiments of Lafaurie et al. [5] yielded poor results. The pronounced effect of rotation generates a large amount of flotsam on large lattices, or spikes were created on the flat surfaces of the rectangle. As seen in Fig. 8, the results of the present advection scheme show that the rectangular shape is better maintained; there is no flotsam seen and the deformation of the rectangular shape is considerably suppressed in comparison of the results of [5].

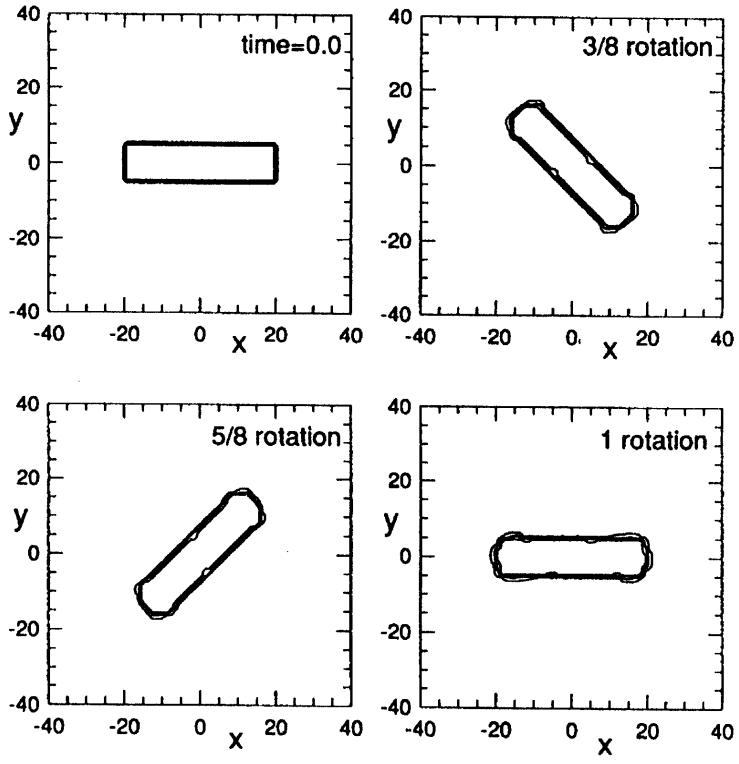


Fig. 8 Rotation of a rectangle.

*4.2 Evolution of Surface Waves*

As shown in Fig. 9, a square cavity is partitioned into two compartments of different heights. Each compartment is filled with a different fluid. At time $t=0$, the entire partition is removed, and the hydrostatic pressure difference derives the flow.

A mesh of 82x82 grid points, with uniform spacing, is used. The height difference to length of the square cavity is $h/L=0.5$. Two calculations are made for two values of density difference, $\rho_2/\rho_1 =0.5$, 0.1, with $R_{\Delta\rho}=2gh^2\rho_1^2/(\rho_1-\rho_2)\mu_1=100$ and $\mu_1/\rho_1=\mu_2/\rho_2$. Fig. 9 depicts the time-dependent fluid interface for $\rho_2/\rho_1=0.5$. The fluid column in the right side collapses to form surface waves due to the initially-stored hydrostatic pressure difference. Fig. 9 shows a breakdown process of the surface wave. The isolated drops and bubbles seen in the lower frames of Fig. 9 could indicate the results of wave breakdown, although no conclusive statements can be made at this stage. Fig. 10 exhibits the results under a more severe condition, $\rho_2/\rho_1=0.1$. In this case, the initially-stored potential energy difference is large enough for the denser fluid to flow up to the upper wall. The fluid, after hitting the upper wall, appears to form a falling drop. It is noted that the present calculations have insufficient resolution to describe the detailed dynamics of drops. However, these tests demonstrate the improved capabilities of the present method of depicting the prominent features of flows of immiscible fluids.

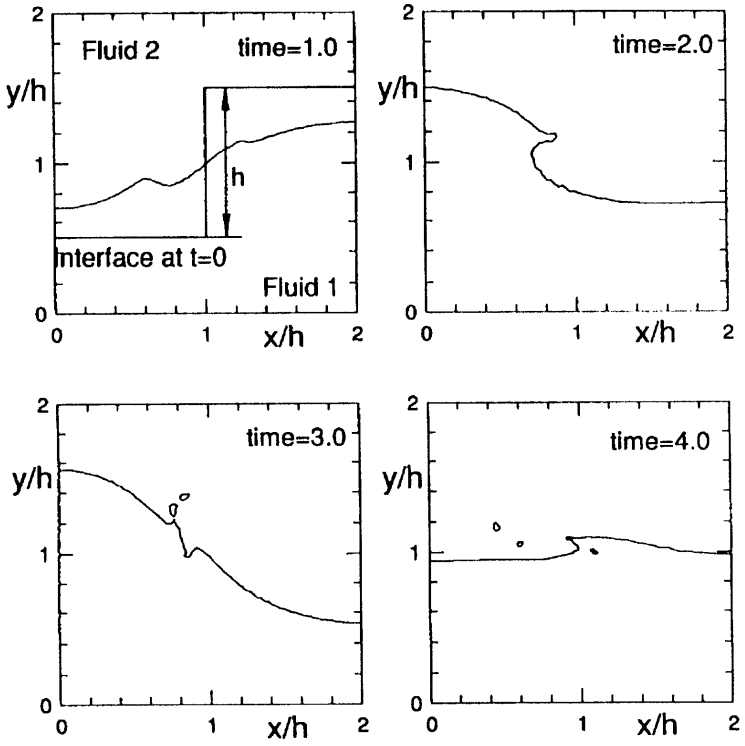


Fig. 9 Time-dependent evolution of the interface for $\rho_2/\rho_1=0.5$.

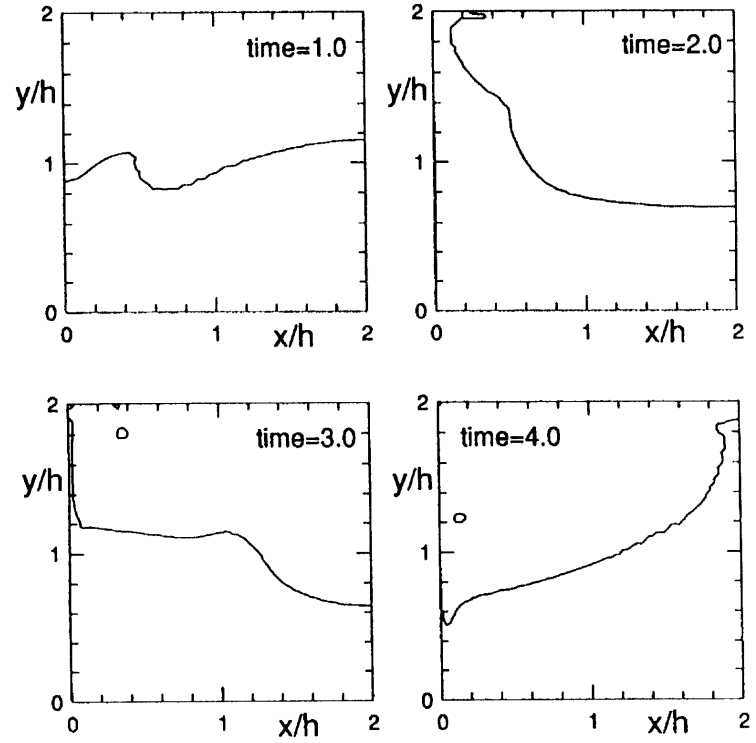


Fig. 10 Time-dependent evolution of the interface for $\rho_2/\rho_1=0.1$.

### *4.3. Spin-Up from Rest of a Two-Layer Liquid in a Cylinder*

The spin-up process of a confined two-layer liquid, due to an impulsive rotation of the cylinder, was treated recently [*11,12*] in an experimental and analytical study. Consider a vertically-mounted cylindrical cavity of radius $R$ and height $H$. At the initial state, two homogeneous, immiscible liquids fill completely the cylinder at rest, and the interface is horizontal at $y=h$. At $t=0$, the cylinder is abruptly set to rotate about its vertical $y$-axis at rotation rate $\Omega$.

In order to facilitate a direct comparison with the preceding results [*11,12*], the parameters are selected as follow: $\rho_1/\rho_2=0.7465$, $\mu_1/\mu_2=0.134$, $H/R=4.54$, $h/H=0.5$. Two calculations are conducted for the Ekman number, $E_1=\mu_1/\rho_1\Omega h^2=1.33\times10^{-2}$ and $E_1=1.33\times10^{-3}$. A mesh of 52x102 grid points is used and the grid is stretched near the solid walls.

Fig. 11 depicts the time-dependent evolution of the interface for $E_1=1.33\times10^{-2}$. At small times, the bottom layer gains angular velocity faster than the top layer, which makes the interface in the central region to recede. Around time $\Omega t=18$, the interface at the centerline reaches the lowest level, and it rises to the final steady-state parabolic profile as time passes. The present results shows a good agreement with the previous results [*11,12*]. Fig. 12 typifies the results of the case under a more faster rotation, $E_1=1.33\times10^{-3}$. Here, note that, for this case, the Ekman number of the upper liquid layer is very small, $E_2=1.33\times10^{-4}$. The usual SOLA-VOF version [*4*] has difficulties in simulating such cases ([*12*] private communication). The results of the present method are stable, and they are in broad agreement with the available experimental data [*11*].

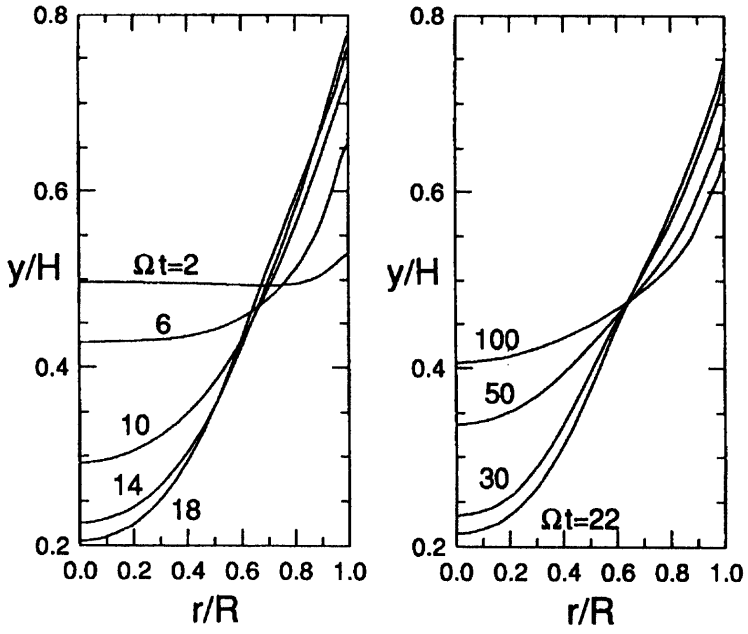


Fig. 11 Sequential plots of the interface in the spin-up process for $E_1=1.33\times10^{-2}$.

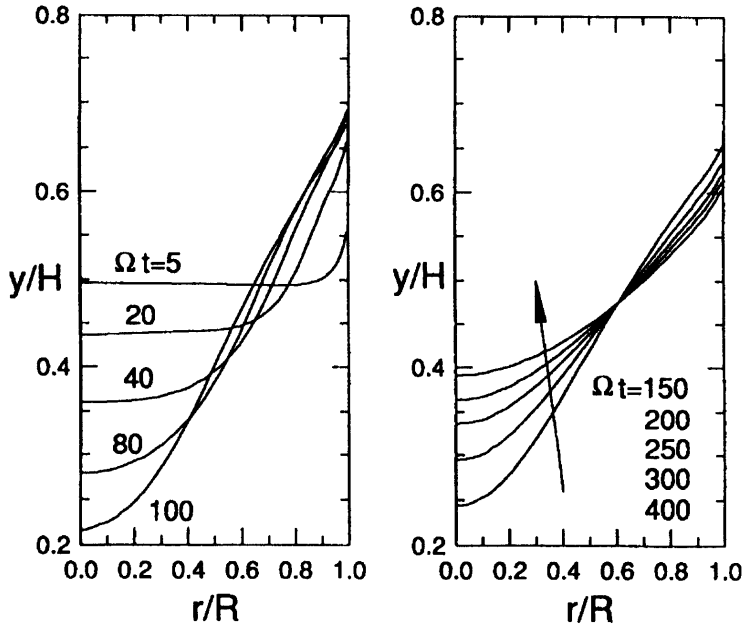


Fig. 12 Sequential plots of the interface in the spin-up process for $E_1=1.33\times10^{-3}$.

## 5. CONCLUDING REMARKS

A numerical algorithm based on VOF has been presented as a means for simulating flows with interface between immiscible fluids. The key element is a new advection scheme for the transport of the volume of fluid, which is designed (i) to take into account the cross-directional upstream effects, and (ii) to be coupled with a generalized the FCT technique [*8*]. The improved time accuracy of this VOF-FCT scheme leads to a better description of the interface motion.

The overall solution algorithm together with the advection scheme was described in detail. Test simulations illustrates several the improved features of the present method and its applicability to simulate a wide range of complicated flows.

This present method was derived for the two-dimensional formulation. It is, however, notable that each step of the solution procedures is fully free from the directional bias. Thus, the extension to the three-dimensional situations is straightforward.

# REFERENCES

[1] HARLOW, F and WELCH, J. E.: Numerical Calculation of Time-Dependent Viscous Incompressible Flow of Fluid with Free Surface, Phys. Fluids vol. 9, 2182-2189 (1865).

[2] TOME, M. F. and MCKEE, S.: GENSMAC: A Computational Marker and Cell Method for Free Surface Flows in General Domain, J. Comput. Phys. vol. 110, pp. 171-186 (1994).

[3] MONAGAN, J. J.: Simulating Free Surface Flows with SPH, J. Comput. Phys. vol. 110, pp. 399-406 (1994).

[4] HIRT, C. W. and NICHOLAS, B. D.: Volume of Fluid (VOF) Method for the Dynamics of Free Boundaries, J. Comput. Phys. vol. 39, pp. 201-225 (1981).

[5] LAFAURIE, B., NARDONE, C., SCARDONELLI, R., ZALESKI, S. and ZANETTI, G.: Modeling Merging and Fragmentation in Multiphase Flows with SUFFER, J. Comput. Phys. vol. 113, pp. 134-147 (1994).

[6] THOMAS, T. G., LESLIE, D. C. and WILLIAMS, J. J. R.: Free Surface Simulations Using a Conservative 3D Code, J. Comput. Phys. vol. 116, pp. 52-68 (1995).

[7] ORAN, E. S. and BORIS, J. P.: Numerical Simulation of Reacting Flows, Elsevier, New York (1987).

[8] ZALESAK, S. T.: Fully Multi-Dimensional Flux-Corrected Transport Algorithms for Fluids, J. Comput. Phys. vol. 31, pp. 335-362 (1979).

[9] BORIS, J. P., GARDNER, J. H., ORAN, E. S., GUIRGUIS, R. H. and PATNAIK, G.: LCPFCT - Flux-Corrected Transport for Generalized Continuity Equations, NRL Memorandum Report, Naval Research Laboratory, Washington, DC (1987).

[10] BORIS, J. P. and BOOKS, D. L.: Flux-Corrected Transport I: SHASTA - A Fluid Transport Algorithm that Works, J. Comp. Phys. vol. 11, pp. 38-69 (1973).

[11] LIM, T. G., CHOI, S. M. and HYUN, J. M.: Transient Interface Shape of a Two-Layer Fluid in an Abruptly Rotating Cylinder, ASME. J. Fluid Engineering, vol. 115, pp. 324-329 (1993).

[12] KIM, K. Y. and HYUN, J. M.: Spin-Up from Rest of a Two-Layer Liquid in a Cylinder, ASME J. Fluid Engineering vol. 116, pp. 808-814 (1994).